Uncertainty Quantification of Density Reconstruction in High-Energy X-ray Radiography

Haibo Xu

Institute of Applied Physics and Computational Mathematics
Beijing, P.R. China
Email: xu_haibo@iapcm.ac.cn

Xinge Li

Institute of Applied Physics and Computational Mathematics
Beijing, P.R. China
Email: lixinge@lsec.cc.ac.cn

***Abstract*—High-energy X-ray radiography is a measuring technique for quantitative diagnosis of the object and its internal structure. Tomographic reconstruction determines the geometric and physical properties of the object according to the energy distribution on the imaging plane. Considering the noise and blur in the process of radiographing, we construct a general reconstruction model for the axisymmetric single image photographic system. This inverse problem is then cast within a statistical framework in order to compute volumetric object densities from X-ray radiographs and to quantify uncertainties in the reconstruction. A hierarchical Bayesian model is developed with a likelihood based on a Gaussian noise model and with priors placed on the unknown nonnegative density profile, the precision matrix, and two scale parameters. This results in a joint posterior distribution, which can be readily sampled using the Markov chain Monte Carlo (MCMC) method. To study the role of hyperparameters and their sensitivity analysis, a wide variety of tests were conducted which led to a number of definitive conclusions. Results of the density reconstructions and pointwise uncertainty estimates are presented for simulated signals with various physical factors in the imaging process included.**

Keywords–inverse problem; density reconstruction; uncertainty quantification; Bayesian inference; MCMC method.

I. INTRODUCTION

High-energy X-ray radiography measures the spatial density distribution of the object, which is of great significance for studying the compression behavior of the object subjected to powerful shocks under the effect of explosives. In this paper, we focus on the problem of uncertainty quantification of density reconstruction for high-energy X-ray radiography. Bayesian formulations for inverse problems have gained considerable attention in the inverse problems community for their utility in uncertainty quantification [1]–[7]. In the application here, we seek an unknown that contains discontinuities but we do not precisely know the discontinuity locations, so we develop a hierarchical Bayesian model for localizing the discontinuities and computing object densities simultaneously. The Bayesian approach combines the prior knowledge of the unknown parameters and the forward model to yield a posterior probability distribution of the model parameters. In this way, the unknown parameters can be characterized by their posterior distributions. The posterior distributions are typically not of analytical form or from a standard parametric family, and characterizing them exactly requires optimization algorithms [8]–[11] or sampling approaches such as MCMC [12].

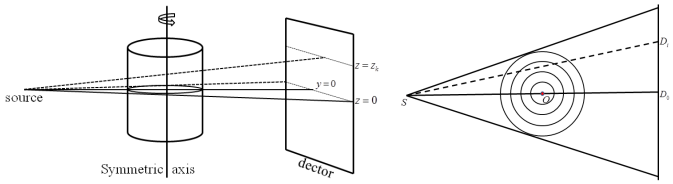

Figure 1. Illustration to single radiographic imaging system for radially symmetric object in 3D view (a) and 2D view (b).

In our experimental setting, a radially symmetric object with radius R and height H is situated so that its center-layer lies in the xy-plane and its axis of symmetry coincides with the z-axis (see Figure 1(a)). Only a single radiograph is taken with a radiographic axis perpendicular to the symmetric axis of the object. The transmitted radiation is measured by a detector lying on a plane $x = x_0$. The X-ray source is placed sufficiently far from the object compared to its size, so that the X-rays can be assumed to be parallel on different layers. In each layer, we consider that the X-rays form a fan-beam shape, see Figure 1(b). Each cross section of the object is projected onto a line of the detector plane. We formulate the density reconstruction model as

$$\mathbf{b} = \mathbf{K}\mathbf{A}\boldsymbol{\rho} + \boldsymbol{\varepsilon}, \tag{1}$$

where $\mathbf{b} \in \mathbb{R}^m$ is the areal density values, $\boldsymbol{\rho} \in \mathbb{R}^n$ is the object radial density values, $\boldsymbol{\varepsilon} \in \mathbb{R}^m$ is unknown noise, $\mathbf{K}$ presents the blurring that may be produced in the process of radiographing, and $\mathbf{A} \in \mathbb{R}^{m\times n}$ denotes the forward projection matrix.

The rest of the paper is organized as follows. Section II discusses how to estimate the object density and its corresponding uncertainty quantitatively. Uncertainty quantification of the French Test Object (FTO) reconstruction are presented in Section III, as well as the parameter selection method and sensitivity study. Finally, the conclusion and outlook are given in Section IV.

II. BAYESIAN FORMULATION OF RECONSTRUCTION PROBLEM

In this section, we introduce a hierarchical Bayesian model to compute object densities and quantify their corresponding

 ISBN: 978-1-61208-737-5

uncertainties at the same time. By selecting conjugate prior distributions, the final posterior formulation can be easily and efficiently sampled using a Gibbs sampler, a specialized MCMC method.

A. Hierarchical Bayesian model

Since the noise distribution in areal density space is difficult to estimate, we begin with the standard additive Gaussian noise model [13], [14], i.e., $\boldsymbol{\varepsilon} \sim \text{Normal}(\mathbf{0}, (\lambda\mathbf{I})^{-1})$ with precision λ. Then the conditional probability density of $\mathbf{b}$ given the information of $\boldsymbol{\rho}$ and λ, would be

$$p(\mathbf{b}|\boldsymbol{\rho}, \lambda) \propto \lambda^{m/2} \exp\left(-\frac{\lambda}{2}\|\mathbf{K}\mathbf{A}\boldsymbol{\rho} - \mathbf{b}\|^2\right). \quad (2)$$

Assume that the prior model for $\boldsymbol{\rho}$ is also a Gaussian,

$$\boldsymbol{\rho} \sim \text{Normal}(\mathbf{0}, (\delta\mathbf{L})^{-1}),$$

where $\mathbf{L} \in \mathbb{R}^{n\times n}$ is referred to as the precision matrix, and $\delta > 0$ and $\mathbf{L}$ are poorly known. Hence, we write a conditional prior for $\boldsymbol{\rho}$, assuming that δ and $\mathbf{L}$ were known, as

$$p(\boldsymbol{\rho}|\delta, \mathbf{L}) \propto \delta^{n/2}|\mathbf{L}|^{1/2} \exp\left(-\frac{\delta}{2}\boldsymbol{\rho}^{\mathrm{T}}\mathbf{L}\boldsymbol{\rho}\right),$$

that is, the prior density is conditioned on the knowledge of δ and $\mathbf{L}$. In consideration of the nonnegativity of density value $\boldsymbol{\rho}$, we impose nonnegativity constraint on the computed samples. Suppose $\mathcal{I} = \mathcal{I}(\boldsymbol{\rho}) \stackrel{\text{def}}{=} \{i|\rho_i = 0\}$ is the zero set and $p(\mathcal{I})$ a probability model for $\mathcal{I}$. Then the prior will depend upon the zero set. If we define $\mathbf{C}$ to be the diagonal matrix with diagonal entries $c_{ii} = 1$ for $i \notin \mathcal{I}$, and $c_{ii} = 0$ otherwise, the prior in the unconstrained case is modified as follows:

$$p(\boldsymbol{\rho}|\delta, \mathbf{L}, \mathcal{I}) \propto \delta^{n_p/2}|\mathbf{L}|^{1/2} \exp\left(-\frac{\delta}{2}\boldsymbol{\rho}^{\mathrm{T}}\mathbf{C}\mathbf{L}\mathbf{C}\boldsymbol{\rho}\right), \quad (3)$$

where $n_p = n - |\mathcal{I}|$, i.e., the number of positive elements in $\boldsymbol{\rho}$.

Assume further that we have a hyperprior density $p(\mathbf{L})$ for the precision matrix $\mathbf{L}$. We suppose here that this density is a Wishart distribution, which is often used for inverse covariance matrices [15]. Thus $\mathbf{L} \sim \text{Wishart}(\Sigma, \nu)$, with probability density function

$$p(\mathbf{L}) = \frac{1}{2^{\nu n/2}|\Sigma|^{\nu/2}\Gamma_n(\nu/2)}|\mathbf{L}|^{\frac{\nu-n-1}{2}} \exp\left(-\frac{1}{2}\text{tr}(\Sigma^{-1}\mathbf{L})\right), \quad (4)$$

where Σ is a positive definite scale matrix, and ν is the degrees of freedom parameter.

Last, a Gamma hyperprior distribution is chosen for both scale parameters λ and δ so that

$$p(\lambda) \propto \lambda^{\alpha_\lambda - 1}\exp(-\beta_\lambda\lambda), \quad (5)$$
$$p(\delta) \propto \delta^{\alpha_\delta - 1}\exp(-\beta_\delta\delta), \quad (6)$$

that is, $\lambda \sim \text{Gamma}(\alpha_\lambda, \beta_\lambda)$, $\delta \sim \text{Gamma}(\alpha_\delta, \beta_\delta)$, where α_λ and α_δ are Gamma shape parameters and β_λ and β_δ are Gamma rate parameters.

Considering now all $\boldsymbol{\rho}$, λ, δ, $\mathbf{L}$ and $\mathcal{I}$ as unknowns, we write Bayes' formula conditioned on $\mathbf{b}$ as

$$p(\boldsymbol{\rho}, \lambda, \delta, \mathbf{L}, \mathcal{I}|\mathbf{b}) \propto p(\mathbf{b}|\boldsymbol{\rho}, \lambda, \mathcal{I})p(\boldsymbol{\rho}|\delta, \mathbf{L}, \mathcal{I})p(\mathbf{L})p(\delta)p(\mathcal{I})p(\lambda),$$

which allows us to estimate $\boldsymbol{\rho}$, λ, δ and $\mathbf{L}$ simultaneously:

$$\boldsymbol{\rho}|\lambda, \delta, \mathbf{L}, \mathcal{I}, \mathbf{b} \sim \text{Normal}(\mathbf{B}_{\mathcal{I}}^{\dagger}\lambda\mathbf{A}^{\mathrm{T}}\mathbf{K}^{\mathrm{T}}\mathbf{b}, \mathbf{B}_{\mathcal{I}}^{\dagger}), \quad (7)$$
$$\lambda|\boldsymbol{\rho}, \delta, \mathbf{L}, \mathcal{I}, \mathbf{b} \sim \text{Gamma}\left(m/2 + \alpha_\lambda, \frac{1}{2}\|\mathbf{K}\mathbf{A}\mathbf{C}\boldsymbol{\rho} - \mathbf{b}\|^2 + \beta_\lambda\right), \quad (8)$$
$$\delta|\boldsymbol{\rho}, \lambda, \mathbf{L}, \mathcal{I}, \mathbf{b} \sim \text{Gamma}\left(n_p/2 + \alpha_\delta, \frac{1}{2}\boldsymbol{\rho}^{\mathrm{T}}\mathbf{L}_{\mathcal{I}}\boldsymbol{\rho} + \beta_\delta\right), \quad (9)$$
$$\mathbf{L}|\boldsymbol{\rho}, \lambda, \delta, \mathcal{I}, \mathbf{b} \sim \text{Wishart}((\Sigma^{-1} + \delta(\boldsymbol{\rho}\boldsymbol{\rho}^{\mathrm{T}})_{\mathcal{I}})^{-1}, \nu + 1), \quad (10)$$

where $\mathbf{B} = \lambda\mathbf{A}^{\mathrm{T}}\mathbf{K}^{\mathrm{T}}\mathbf{K}\mathbf{A} + \delta\mathbf{L}$, $\mathbf{D}_{\mathcal{I}} \stackrel{\text{def}}{=} \mathbf{C}\mathbf{D}\mathbf{C}$ and $\dagger$ denotes psuedo-inverse. Since $\mathbf{C}\boldsymbol{\rho} = \boldsymbol{\rho}$ (recall that $\rho_i = 0$ for $i \in \mathcal{I}$), equivalent distributions result if $\mathbf{C}$ is removed in (8), $\mathbf{L}_{\mathcal{I}}$ is replaced by $\mathbf{L}$ in (9), and $(\boldsymbol{\rho}\boldsymbol{\rho}^{\mathrm{T}})_{\mathcal{I}}$ is substituted as $\boldsymbol{\rho}\boldsymbol{\rho}^{\mathrm{T}}$ in (10). We do this in what follows.

It remains to define $p(\mathcal{I})$ and the conditional density $p(\mathcal{I}|\boldsymbol{\rho}, \lambda, \delta, \mathbf{L}, \mathbf{b})$. This can be accomplished by computing [1]

$$\hat{\boldsymbol{\rho}} = \arg\min_{\boldsymbol{\rho}\geq\mathbf{0}}\left\{\frac{1}{2}\boldsymbol{\rho}^{\mathrm{T}}\mathbf{B}\boldsymbol{\rho} - \boldsymbol{\rho}^{\mathrm{T}}(\lambda\mathbf{A}^{\mathrm{T}}\mathbf{K}^{\mathrm{T}}\mathbf{b} + \mathbf{w})\right\}, \quad (11)$$

where $\mathbf{w} \sim \text{Normal}(\mathbf{0}, \mathbf{B})$. That is, solving (11) yields simultaneous samples of both $\boldsymbol{\rho}$ and, implicitly, $\mathcal{I}$ from $p(\mathcal{I}|\boldsymbol{\rho}, \lambda, \delta, \mathbf{L}, \mathbf{b})$. And, more remarkable, this optimization problem can be easily solved exploiting the Constrained Conjugate Gradient (CCG) method [16]. We still have not defined $p(\mathcal{I})$, but this is not necessary to define our MCMC method.

B. MCMC sampling of the posterior distribution

The power in (7)–(10) lies in the fact that samples from these four distributions can be easily computed using standard statistical software, though nonlinear optimization techniques will be needed for (7). A Gibbs sampler that results from sequential use of the conditional densities $p(\mathcal{I}|\boldsymbol{\rho}, \lambda, \delta, \mathbf{L}, \mathbf{b})$ and (7)–(10) can be written without an explicit sampling step for $\mathcal{I}$. The sampler begins with $\boldsymbol{\rho}$, and is initialized with λ_0, δ_0, and $\mathbf{L}_0$. A basic outline is listed in Algorithm 1.

Algorithm 1 (MCMC sampler)

1. Select λ_0, δ_0 and $\mathbf{L}_0$. Select a maximum number of samples, N, and set $k = 0$.
2. Compute
$$\boldsymbol{\rho}^k = \arg\min_{\boldsymbol{\rho}\geq\mathbf{0}}\left\{\frac{1}{2}\boldsymbol{\rho}^{\mathrm{T}}\mathbf{B}_k\boldsymbol{\rho} - \boldsymbol{\rho}^{\mathrm{T}}(\lambda_k\mathbf{A}^{\mathrm{T}}\mathbf{K}^{\mathrm{T}}\mathbf{b} + \mathbf{w})\right\},$$
where $\mathbf{B}_k = \lambda_k\mathbf{A}^{\mathrm{T}}\mathbf{K}^{\mathrm{T}}\mathbf{K}\mathbf{A} + \delta_k\mathbf{L}_k$ and $\mathbf{w} \sim \text{Normal}(\mathbf{0}, \mathbf{B}_k)$, using the CCG method.
3. Compute $\lambda_{k+1} \sim \text{Gamma}(m/2 + \alpha_\lambda, \frac{1}{2}\|\mathbf{K}\mathbf{A}\boldsymbol{\rho}^k - \mathbf{b}\|^2 + \beta_\lambda)$.
4. Compute $\delta_{k+1} \sim \text{Gamma}\left(n_p^k/2 + \alpha_\delta, \frac{1}{2}(\boldsymbol{\rho}^k)^{\mathrm{T}}\mathbf{L}_k\boldsymbol{\rho}^k + \beta_\delta\right)$, where n_p^k is the number of positive entries in $\boldsymbol{\rho}^k$.
5. Compute
$$\mathbf{L}_{k+1} \sim \text{Wishart}\left((\Sigma^{-1} + \delta_{k+1}\boldsymbol{\rho}^k(\boldsymbol{\rho}^k)^{\mathrm{T}})^{-1}, \nu + 1\right).$$
6. Set $k = k + 1$. If $k < N$, return to step 2.

Samples obtained via the above MCMC algorithm are used to compute the sample mean and 95% credibility intervals. The sample mean well characterizes the unknown true density, and the credibility intervals provide uncertainty quantification in the posterior estimate.

 ISBN: 978-1-61208-737-5

III. NUMERICAL EXPERIMENTS

In this section, we test on a simulated radiograph of the FTO, which is generated by the Monte Carlo N-Particle (MCNP) transport code [17], to demonstrate the ability of MCMC method to reconstruct an axially symmetric object. In this numerical simulation, the source is assumed as a monoenergetic photon beam of $4\,\text{MeV}$, and the source blur is treated as Gaussian, whose full width at half maximum is $0.3\,\text{cm}$. The FTO consists of a set of concentric spheres with a void region at the center. The void has a radius of $1.0\,\text{cm}$. The second layer is tungsten with radius of $4.5\,\text{cm}$ and density of $18.9\,\text{g/cm}^3$. The third layer is copper with radius of $6.5\,\text{cm}$ and density of $8.9\,\text{g/cm}^3$. The FTO is placed $200\,\text{cm}$ from the source, and the detector is $250\,\text{cm}$ behind the object. Figure 2(a) shows the synthetic radiograph of the total exposure, and Figure 2(b) shows the profiles at the equator of the direct and scattered exposure respectively.

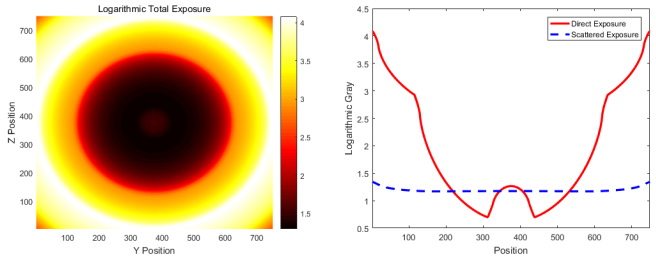

(a) (b)

Figure 2. MCNP simulation results of the FTO. (a) Radiograph capturing both direct and scattered radiation; (b) the central cross sections of the direct and scattered exposure.

Obviously, the introduction of the hyperprior distributions in (4)–(6) requires the choice of hyperparameters α_λ, β_λ, α_δ, β_δ, ν, and Σ. Setting the MCMC sampler with these hyperparameters and initializations λ_0, δ_0 and $\mathbf{L}_0$, we computed 100,000 samples and made the last 95,000 available, which demonstrated stationarity and had little correlation between samples [15]. From these samples, we plot the sample mean as our reconstruction, which is known as conditional mean (CM) estimate of the unknown density, and 95% credibility intervals given by the 0.025 and 0.975 quantiles of the samples at each location, which were computed using empirical quantiles.

A. Parameter selection

We have to study first the role of hyperparameters. For the hyperparameters $(\alpha_\lambda, \beta_\lambda)$, it is easy to see that λ characterises the noise level σ^2 of areal density. The smaller the value, the higher the noise. Since the mean and variance of the corresponding Gamma distribution are $\alpha_\lambda/\beta_\lambda$ and $\alpha_\lambda/\beta_\lambda^2$ respectively, we choose appropriate α_λ and β_λ such that $\alpha_\lambda/\beta_\lambda$ is close to σ^{-2} and $\alpha_\lambda/\beta_\lambda^2$ is smaller. In our numerical experiments, we just set $\alpha_\lambda = \sigma^{-2}$ and $\beta_\lambda = 1$.

We now study the effect of the hyperparameters $(\alpha_\delta, \beta_\delta)$. To this end, we employ the variable-controlling approach by setting λ and $\mathbf{L}$ as known. We then fix $\alpha_\delta = 1$, and the corresponding Gamma distribution degenerates to an exponential distribution. The maximum a posteriori estimate for the pair $(\boldsymbol{\rho}, \delta)$ are calculated for various values of β_δ. We then pick a proper $\hat{\beta}_\delta$ with good performance of $\hat{\boldsymbol{\rho}}$. Similar to λ, we select suitable α_δ and β_δ such that $\alpha_\delta/\beta_\delta$ is equal to $1/\hat{\beta}_\delta$ and $\alpha_\delta/\beta_\delta^2$ is smaller. In our numerical experiments, we just set $\alpha_\delta = \hat{\beta}_\delta^{-1}$ and $\beta_\delta = 1$.

Last but not least, setting the Wishart degrees of freedom parameter $\nu = n + 1$ ensures that the distribution is well defined [18] [19]. Since the Wishart has mean $\nu\Sigma$, the quality of the final reconstruction is supposed to be greatly improved by choosing a Σ that incorporates edge information. We then set $\Sigma = \frac{1}{\nu}\mathbf{L}_{\text{TV}}(\boldsymbol{\rho}_{\text{TV}})$ to center the hyperprior for $\mathbf{L}$ around the initial edge estimate provided by total variation (TV) solution $\boldsymbol{\rho}_{\text{TV}}$, where $\mathbf{L}_{\text{TV}}(\boldsymbol{\rho}_{\text{TV}}) = \mathbf{D}^{\text{T}}\psi(\boldsymbol{\rho}_{\text{TV}})\mathbf{D}$, $\psi(\boldsymbol{\rho}_{\text{TV}}) := \text{diag}\left(1/\sqrt{(\mathbf{D}\boldsymbol{\rho}_{\text{TV}})^2 + \eta}\right)$, η is a small positive constant, and $\mathbf{D}$ is the forward differencing matrix [15].

B. Parameter sensitivity

We now reconstruct the density distribution of the FTO with the resulting areal density from the direct radiation shown in Figure 2(b), and provide a parameter sensitivity analysis for Σ and β_δ. For the MCMC sampler, the degrees of freedom parameter ν is set to be $n + 1$, the Wishart scale matrix Σ is computed to be $\frac{1}{\nu}\mathbf{L}_{\text{TV}}(\boldsymbol{\rho}_{\text{TV}})$, and $\mathbf{L}_{\text{TV}}(\boldsymbol{\rho}_{\text{TV}})$ is also used for $\mathbf{L}_0$. The initial λ and δ parameters are drawn from a Uniform$(0, 1)$ distribution. All the remaining parameters for the Gibbs sampler are selected as noted above and are given in Table I.

The sensitivity of the TV solution, which is used to inform the hyperparameter Σ, is tested by providing the sampler with a TV solution that contained no edge information and a TV solution that indicated incorrect edge locations and densities. For ease of comparison, we also calculate the CM estimate, initializing the sampler with a proper TV solution. The mean square error is computed using the mean reconstruction compared to the true density profile of the FTO. As shown in Table I, the mean square error of the original reconstruction is 0.0637392 and each of these two reconstructions differs from that by no more than 0.000002. Both of these reconstructions demonstrate the Bayesian method's ability to overcome a poorly informed Σ parameter, relying on the data to determine edges and density scales.

To understand the sensitivity of the solution to the parameter β_δ, we carry out reconstruction experiments on the areal density, which is corrupted with Gaussian noise at level 1.5% of maximum of the noiseless projection data. Samples of the MCMC chain are drawn from the conditional distributions, holding all but β_δ constant and changing β_δ from 10^0 to 10^1. Combined with the mean square error in Table I, we can observe that the MCMC sampler with different β_δ makes very little difference.

TABLE I. PARAMETERS STATISTICS AND COMPARISON OF MEAN SQUARE ERRORS.

α_λ	β_λ	α_δ	β_δ	Σ	$\|\boldsymbol{\rho}_{\text{MCMC}} - \boldsymbol{\rho}_{\text{true}}\|/\sqrt{n}$
10^6	10^0	10^2	10^0	correct	0.0637392
10^6	10^0	10^2	10^0	non	0.0637399
10^6	10^0	10^2	10^0	wrong	0.0637404
7.3×10^5	10^0	10^2	10^0	correct	0.0636181
7.3×10^5	10^0	10^2	10^1	correct	0.0632581

We can summarize from the data in Table I that $(\alpha_\delta, \beta_\delta)$ can be applicable to the projection data of the same object in different situations, while the selection of $(\alpha_\lambda, \beta_\lambda)$ is related

 ISBN: 978-1-61208-737-5

to the noise level of the projected data, and different values are obtained for different data.

C. Uncertainty caused by physical factors

Although empirical knowledge constraints have been added into density reconstruction, it does not eliminate the uncertainty of reconstruction results (11), but only reduces the uncertainty of reconstruction modeling (1), so it is necessary to analyze the factors causing uncertainty in density reconstruction. Generally, there are uncertainties caused by the conversion from optical density to areal density, the noise in areal density, the measurement error of areal density as well as the reconstruction method itself. In our simulation, errors in the reconstruction from the direct radiation data are mainly caused by the noise and measurement error in areal density and our approach to the density reconstruction problem (1).

Images captured by X-ray imaging systems are direct measures of the optical density. The measured optical density, G, can be converted to areal density, b, using a measured transmission curve, which is given by

$$G = G_0 + k(X_D + X_S) = G_0 + k\left(\frac{X_0}{d^2}e^{-b} + X_S\right), \quad (12)$$

where G and G_0 is the optical density and background density at that point; k is the slope of the transmission curve; X_0 is the radiation exposure; d is the distance between source and the imaging plane; X_S is the scattered radiation; X_D is the direct radiation. The uncertainty of areal density measurement caused by the indeterminacy of scattering irradiation, incident exposure and transmission curve measurements can be summarized as

$$\Delta b = \sqrt{\mathrm{SDR}^2\left(\frac{\Delta X_S}{X_S}\right)^2 + \left(\frac{\Delta X_0}{X_0}\right)^2 + (1+\mathrm{SDR})^2\left(\frac{\Delta k}{k}\right)^2}, \quad (13)$$

where $\mathrm{SDR} = \frac{X_S}{X_D}$ denotes the ratio of scattering to direct radiation. According to the accuracy of experimental measurement, the error range of physical quantities in (13) can be approximated by

$$\frac{\Delta X_S}{X_S} \le 10\%, \quad \frac{\Delta X_0}{X_0} \le 5\%, \quad \frac{\Delta k}{k} \le 10\%,$$

then we can obtain the measurement error of areal density:

$$\Delta b = 0.1\sqrt{\mathrm{SDR}^2 + 0.25 + (1+\mathrm{SDR})^2}. \quad (14)$$

To analyse the uncertainty introduced by noise in the imaging process, we carry out reconstruction experiment on the noisy areal density, which is corrupted with Gaussian noise at level 1.5% of maximum of the noiseless projection data. Compared with the posterior estimation from noiseless data, as shown in Figure 3 (a), credibility interval at every location in (b) becomes obvious when noise added, and all of them are within 10% of the density value there. When comparing the CM estimate with TV estimate, in the terminology of the classical regularization theory one is tempted to say that the former is underregularized compared to the latter. However, from the statistical point of view, the CM estimate is consistent with the prior.

In consideration of the uncertainty in areal density measurement, we impose the correct value Δb on the areal density. Then we run MCMC for the corrected areal densities $b - \Delta b$ and $b + \Delta b$ separately. To imitate the density uncertainty caused by measurement uncertainty, these two estimates are merged into single one, as shown in Figure 3 (c), whose density values are average of two estimates, and the pointwise credibility intervals are unions of two original intervals. The mean square error between the density distributions in (c) and (a) is 0.0133972, which verifies the validity of our estimation method. The credible band is tight across the image except for the jump locations.

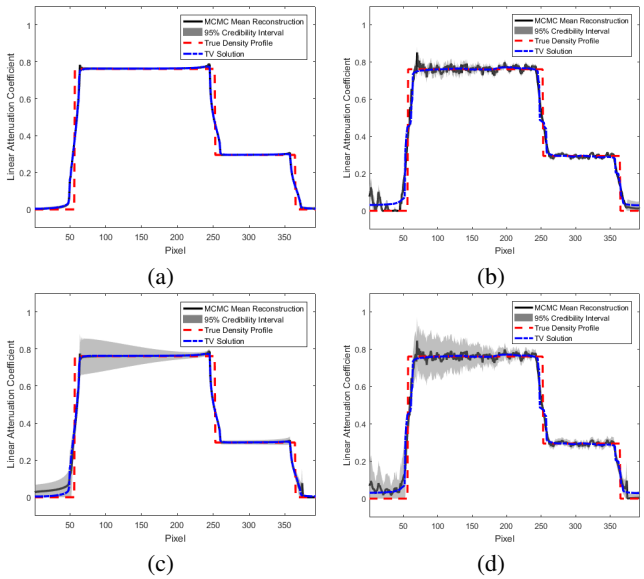

Figure 3. Density reconstructions. (a) Reconstruction results from the noiseless areal density; (b) reconstruction results from the noisy areal density; (c) reconstruction results from the noiseless areal density with correction; (d) reconstruction results from the noisy areal density with correction.

Considering the uncertainties caused by noise and areal density measurement together, we get the noisy areal density to minus and plus the correction (14) separately, and obtain the corresponding noisy projection data with correction. Based on the previously explained MCMC run, the CM estimates together with credible intervals are shown in Figure 3 (d). It is easy to see that the density distribution in (d) is very close to those in (b), and the mean square error between them is 0.0130941. However, the 95% credibility intervals become wider with the introduction of correction, particularly around the boundary of inner layers, and this is consistant with the case in (c). In each example illustrated above, the uncertainty is seen to be lower near regions of constant density in the reconstruction and higher near edge locations.

IV. Conclusion

In this paper, a generalized density reconstruction model is presented based on the assumption that noise and blur will occur during the imaging process. Then, a hierarchical Bayesian model is proposed for computing object densities and estimating their uncertainties simultaneously. Density samples drawn from the conditional posterior distribution are insensitive to the choice in hyperparameter values selected based on the model. Numerical experiments indicate that our MCMC method achieves quite effective reconstruction results and is comparable to TV regularization. Moreover, the uncertainty

 ISBN: 978-1-61208-737-5

of density reconstruction is mainly introduced by noise and measurement error of physical quantities in the process of radiography.

In this paper, the X-rays are assumed to be parallel on different layers, and they form a fan-beam shape in each layer. In the future, we plan to estimate the uncertainty of cone beam reconstruction using the MCMC method. Furthermore, we will consider other explicit noise models according to the characteristics of experimental data, such as poisson noise, impulse noise and a composition of them. We will also construct the prior density in more ways based on the nature of the prior information, for example, ℓ^1 prior, Cauchy density, entropy density, lognormal density, discontinuities prior and so on.

ACKNOWLEDGMENT

H. Xu was supported by NSFC Funds (grant No. 11675021). X. Li was supported by National Postdoctoral Program for Innovative Talents (grant No. BX201700038).

REFERENCES

[1] J. M. Bardsley and C. Fox, "An MCMC method for uncertainty quantification in nonnegativity constrained inverse problems," *Inverse Problems in Science & Engineering*, vol. 20, no. 4, pp. 477–498, 2012.

[2] J. P. Kaipio and E. Somersalo, "Statistical and computational inverse problems," *Technometrics*, vol. 48, no. 1, pp. 146–146, 2005.

[3] A. M. Stuart, "Inverse problems: A Bayesian perspective," *Acta Numerica*, vol. 19, no. 19, pp. 451–559, 2010.

[4] L. Tenorio, *Statistical Regularization of Inverse Problems*. Society for Industrial and Applied Mathematics, 2001.

[5] J. Li and Y. M. Marzouk, "Adaptive construction of surrogates for the bayesian solution of inverse problems," *SIAM Journal on Scientific Computing*, vol. 36, no. 3, pp. A1163–A1186, 2014.

[6] L. Yan and T. Zhou, "Adaptive multi-fidelity polynomial chaos approach to bayesian inference in inverse problems," *Journal of Computational Physics*, vol. 381, pp. 110–128, 2019.

[7] L. M. M. V. D. Bos, B. Sanderse, W. A. A. M. Bierbooms, and G. J. W. V. Bussel, "Bayesian model calibration with interpolating polynomials based on adaptively weighted leja nodes," *Communications in Computational Physics*, 2019.

[8] A. Soares, R. Rabelo, and A. Delbem, "Optimization based on phylogram analysis," *Expert Systems with Applications*, vol. 78, pp. 32–50, 2017.

[9] M. Shams, E. Rashedi, S. M. Dashti, A. Hakimi, M. Shams, E. Rashedi, S. M. Dashti, and A. Hakimi, "Ideal gas optimization algorithm," *International Journal of Artificial Intelligence*, vol. 15, no. 2, pp. 116–130, 2017.

[10] R.-E. Precup, *Nature-Inspired Optimization Algorithms for Fuzzy Controlled Servo Systems*. Oxford: Butterworth-Heinemann, 2019.

[11] B. H. Abed-alguni, "Island-based cuckoo search with highly disruptive polynomial mutation," *International Journal of Artificial Intelligence*, vol. 17, no. 1, pp. 1–29, 2019.

[12] S. Brooks, A. Gelman, G. L. Jones, and X.-L. Meng, *Handbook of Markov Chain Monte Carlo*. Boca Raton: Chapman & Hall/CRC, 2011.

[13] D. Calvetti and E. Somersalo, *Introduction to Bayesian scientific computing*. New York: Springer, 2007.

[14] O. Scherzer, M. Grasmair, H. Grossauer, M. Haltmeier, and F. Lenzen, *Variational Methods in Imaging*. New York: Springer, 2009.

[15] M. Howard, M. Fowler, A. Luttman, S. E. Mitchell, and M. C. Hock, "Bayesian Abel inversion in quantitative X-ray radiography," *SIAM Journal on Scientific Computing*, vol. 38, no. 3, pp. B396–B413, 2016.

[16] E. A. H. Vollebregt, "The bound-constrained conjugate gradient method for non-negative matrices," *Journal of Optimization Theory and Applications*, vol. 162, no. 3, pp. 931–953, 2014.

[17] X. M. C. Team, "MCNP – A general Monte Carlo N-particle transport code, version 5," Los Alamos Nuclear Laboratory, Tech. Rep. LA-UR-03-1987, 2003.

[18] C. Bishop, *Pattern Recognition and Machine Learning*. New York: Springer, 2006.

[19] A. Gelman *et al.*, *Bayesian Data Analysis*. Boca Raton: CRC Press, 2013.

 ISBN: 978-1-61208-737-5